Comparison of Directionally Solidified Samples Solidified Terrestrially and Aboard the International Space Station

S. Angart, M. Lauer, S.N. Tewari, R.N. Grugel, and D.R. Poirier

Abstract

This article reports research that has been carried out under the aegis of NASA as part of a collaboration between ESA and NASA for solidification experiments on the International Space Station (ISS). The focus has been on the effect of convection on the microstructural evolution and macrosegregation in hypoeutectic Al-Si alloys during directional solidification (DS). Terrestrial DS-experiments have been carried out at Cleveland State University (CSU) and under microgravity on the International Space Station (ISS). The thermal processing-history of the experiments is well defined for both the terrestrially processed samples and the ISS-processed samples. As of this writing, two dendritic metrics was measured: primary dendrite arm spacings and primary dendrite trunk diameters. We have observed that these dendrite-metrics of two samples grown in the microgravity environment show good agreements with models based on diffusion controlled growth and diffusion controlled ripening, respectively. The gravity-driven convection (i.e., thermosolutal convection) in terrestrially grown samples has the effect of decreasing the primary dendrite arm spacings and causes macrosegregation. Dendrite trunk diameters also show differences between the earth- and space-grown samples. In order to process DS-samples aboard the ISS, the dendritic seed crystals were partially remelted in a stationary thermal gradient before the DS was carried out. Microstructural changes and macrosegregation effects during this period are described and have modeled.

S. Angart, Graduate Research Assistant, M. Lauer, Graduate Research Associate, and D.R. Poirier, Professor, are at The University of Arizona; S.N. Tewari, Professor, is at Cleveland State University; R.N. Grugel, Metallurgical Engineer, is at NASA-Marshall Space Flight Center.

Introduction

In recent years, the European Space Agency (ESA) has been conducting experiments on alloy solidification in microgravity. This has included a collaboration with NASA for three directional solidification (DS) experiments aboard the International Space Station (ISS) denoted as MICAST6, MICAST7 and MICAST12. The first two were processed on the ISS in 2009 and 2010; the sample-cartridge-assemblies (SCA) were returned to earth, and researchers at The University of Arizona (UA) and Cleveland State University (CSU) have studied the resulting alloy samples. MICAST12 was processed aboard the ISS in the spring of 2014; the resulting sample has yet to be returned to earth for analysis. The subject alloy for the three experiments has been Al-7 wt.% Si alloy.

Ground-based research by this group and others has demonstrated that directional solidification (DS) of hypoeutectic Al-Si and Al-Cu alloys in normal gravity (1-g) often results in "steepling"-macrosegregation caused by thermosolutal convection. Steepling is a type of macrosegregation in which the periphery of a DS-ed sample is of eutectic composition and is seen in alloys with solutes that increase the density of the liquid during solidification. Computer simulations have also been conducted to complement the experimental research.

These simulations also show the steepling flows and agree well with the radial segregation of the solute in transverse sections taken from cylindrical samples (approximately 8–10 mm diameter). Simulations of the same alloys processed in microgravity (approximated as 0-g) showed that the convection is mitigated significantly because of the lack of buoyancy forces acting on the liquid as the alloys solidify. In 0-g, the only convection is that which satisfies solidification-shrinkage flows, assuming no Marangoni flow at free surfaces. In the two samples that have been returned to earth and studied to date, there is hardly any radial segregation and steepling (with one exception to be discussed).

Another aspect of the research is to study the connection between the gravity-driven convection and the metrics of the dendritic array that form during DS. The metrics include primary dendrite arm spacing (λ_1), tertiary dendrite arm spacing, and primary trunk diameter.

Huang et al. [1] studied the influence of flow, transverse to the growth direction, on the dendrite-tip shape and side-branch length in thin (≈ 200 μm) succinonitrile "alloy" samples. They surmised that the transverse-flow reduces λ_1.

There has been only one prior study involving DS of a space-grown alloy [2]. These researchers solidified Al-26.5 Cu alloy at 4.2 μm s^{-1} in thermal gradients of 25-30 K cm^{-1}. Copper increases the density of the liquid so when terrestrially grown vertically in the usual configuration of gravity pointing downward, and there was severe steepling and a non-uniform dendritic structure. The same alloy grown upside-down exhibited no steepling, and the dendritic structure was uniform. In the microgravity environment, λ_1 was about three times larger than in the counterpart terrestrial-samples. Indeed, we have seen that both λ_1 and the dendrite trunk diameters of space-grown samples follow closely to the models of dendritic growth in a diffusion-controlled field (i.e., no convection), whereas the same metrics in samples terrestrially solidified at slower solidification velocities differ significantly from those grown in 0-g. In particular, the 1-g samples with strong thermosolutal convection and its attendant steepling show much greater differences in the dendritic metrics than do the same metrics for diffusion-controlled transport phenomena. Thus, taken together, the 0-g and 1-g samples present a wide range of thermosolutal convection conditions.

The results of this research are of scientific interest to both solidification researchers and casting practitioners. Understanding the microstructural anomalies caused by convective flows is crucial in

improving the processes used to produce DS- and monocrystal-castings of Ni-based superalloys. The research reported herein is on alloy-samples grown in a simple mold with a uniform diameter of 7.8 mm. Not reported in this article, our DS-research has expanded to include effects of changes in cross-sections. Some of the mono-crystal castings contain micro-struts and micro-beams that are cast in situ and present changes in cross-sectional areas. This research promises to elucidate the role of convection in the formation of defects, and in combination with computer simulations the experiments will enable us to differentiate the detrimental effects of thermosolutal convection, which is gravity-dependent, and of the shrinkage-driven convection, which is gravity-independent. Understanding the convective phenomena is an important step toward the continual quest to improve engineering methodology to better design casting-features and processes to mitigate defects in DS-castings.

Furnace on the International Space Station and Alloy-Sample Preparation

Figure 1 shows the Microgravity Science Research Facility (MSRF) on the International Space Station. It is designed to accept various modules that are used for experiments in the physical sciences. It serves to power the modules and interface with the ISS for accepting and recording electronic measurements. On the middle right, the shiny circular component is a door of a chamber that accepts the Bridgman-type furnace that was used for the subject-samples discussed in this article. A drawing of the furnace, which is referred to as the Low Gradient Furnace (LGF), is shown in Fig. 2. Power leads extend from the furnace that connect to heaters in the hot-zone (hot cavity) and to heaters in the cold-zone (cold cavity). The furnace, which is referred to as the Low Gradient Furnace (LGF), is shown in Fig. 2. Power leads extend from the furnace that connects to heaters in the hot-zone and to heaters in the cold-zone. In this research, only the hot-zone was powered; the heaters in the cold-zone were not utilized. Figure 3 shows a Sample Cartridge Assembly (SCA), which contained the alloy to be directionally solidified. The Al-7Si alloy, itself, had a diameter of 7.8 mm and was about 24 cm in length. The samples of the subject-alloy were prepared as dendritic monocrystals by directional solidification at Cleveland State University, where they were carefully machined in preparation for assembling into the SCA's by a company contracted by ESA. The samples were fit into high-purity alumina tubes and encapsulated into the tantalum tubes shown in Fig. 3. The compartment at the end of the Ta-tube assembly is for interfacing with the MSRF. In the DS-experiments of this article, there were thermocouples positioned along the outside surface of the alumina tubes and additional thermocouples for the heaters. The thermocouple-outputs were wired in the compartment. In addition, the system was equipped so that the SCA's could be evacuated to low vacuum and partially filled with an inert gas for leak detection.

At CSU, the directional solidification was carried out in graphite molds (Fig. 4) that were inductively heated with a high frequency electromagnetic coil. The outside and inside diameters of the graphite crucible-mold were ~ 19 mm and ~ 9 mm, respectively. The graphite mold was inside a quartz tube connected to a vacuum system that achieved a pressure of ≈ 10-4 torr. On the outside of the graphite tube, thermocouples were affixed so that the thermal field could be recorded during the DS. This furnace and set-up were used to prepare the dendritic mono-crystals that were machined and fit into the SCA's for the ISS-experiments and for the earth-grown samples that were directionally solidified. A transverse section of a dendritic monocrystal DS-ed at CSU and was used as a seed crystal for one of the ISS-samples is shown as Fig. 5.

Figure 1: Microgravity Science Research Facility on the International Space Station.

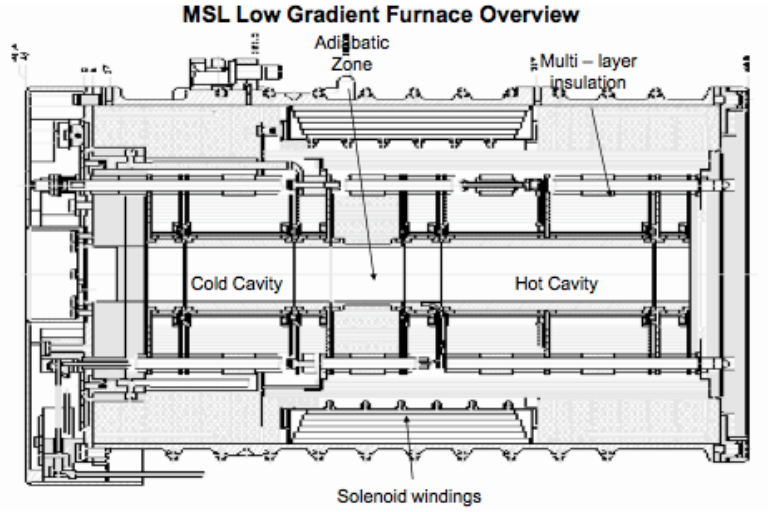

Figure 2: Schematic of Low Gradient Furnace (LGF) used for the directional solidification of MICAST6.

Figure 3: Sample Cartridge Assembly (SCA), in which a sample for a directional solidification experiment on the ISS is contained.

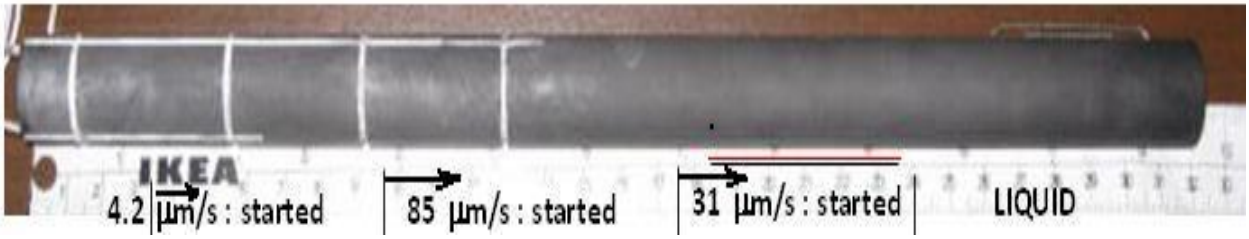

Figure 4: Graphite crucible mold used for solidification of terrestrial samples. The graphite has an inside and outside diameter of ~ 9 mm and ~ 19 mm, respectively.

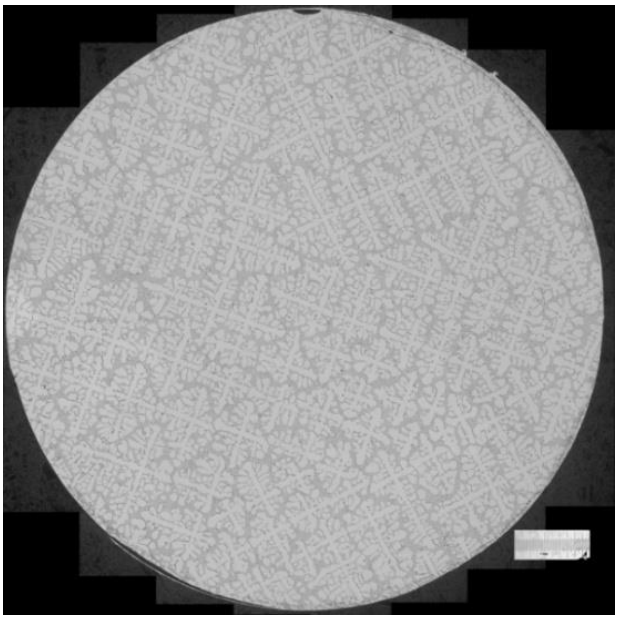

Figure 5: Transverse section of a crystal made at CSU with a solidification velocity of 22 µm s^{-1} in a thermal gradient of 41 $^{o}C\ cm^{-1}$. This sample was used as the seed crystal for MICAST6.

Processing on the International Space Station

When preparing the experiment denoted as MICAST6, the heaters in the hot zone were powered to bring its temperature up to a maximum of 750 ^{o}C and to achieve a thermal gradient aimed at 20 ^{o}C cm^{-1}. A maximum of 750 ^{o}C was selected because previous terrestrial experiments showed that the Al-7Si alloy and the alumina had an unknown reaction above 750 ^{o}C. The gradient of 20 ^{o}C cm^{-1} was a result of putting a limit on the temperature in the hot-zone. Heaters in the cold-zone were not powered. Power settings for the hot-zone heaters had been determined earlier by operating a similar furnace at an ESA-facility. Bringing the furnace to the desired temperature distribution took about one hour. Then the SCA was inserted into the furnace to a predetermined position in order to establish a mushy zone located in the adiabatic zone of the LGF.

The furnace and SCA were held in their positions in order to partially melt the seed crystal and to stabilize the temperatures in the SCA. This pre-DS period was about 5 hrs. for MICAST6. Then DS commenced with the furnace withdrawal rate set at 5 μm s^{-1} for 2.11 hrs, and then the withdrawal rate was changed to 50 μm s^{-1}. During all of this time, thermocouples gathered data at a rate of 1 Hz; these data were subsequently reduced to provide solidification rates, thermal gradients and mushy-zone widths.

The processing schedule of MICAST6 can be seen in Fig. 6, in which the velocities of the nominal liquidus temperature and the solidus temperature (i.e., eutectic temperature) are plotted versus their respective positions. During the pre-DS period, when partial melt back occurred and power settings of heaters in the hot zone were adjusted, the velocities of the two reference temperatures are negative. DS began where the curves are positive. The change to the greater withdrawal rate can be seen where the curves rise. Although the furnace withdrawal rate was constant at 50 μm s^{-1}, notice that the velocities of the solidus and liquidus isotherms never achieved constant values. Post-solidification, Fig. 6 was used to track the solidification rate of the sample (MICAST6) versus distance along its length. The thermocouple data were also reduced to present the thermal gradients measured at the liquidus and eutectic temperatures. These curves for MICAST6 are plotted as Fig. 7 during the DS-period. The thermal gradient at the liquidus is somewhat higher than the gradient at the solidus. When the withdrawal rate was 5 μm s^{-1}, the gradient at the liquidus was 21 to 23 K cm^{-1} while that at the solidus was about 17 to 18 K cm^{-1}. Starting when the withdrawal rate was abruptly increased to 50 μm s^{-1}, the gradients gradually decreased to 19 K cm^{-1} and 17 K cm^{-1}, respectively.

MICAST7 was processed in the Solidification Quench Furnace (SQF), which is also a Bridgman-type furnace that had been employed by ESA-researchers for solidification experiments that did not involve directional solidification. The decision was made to use the SQF because somewhat greater thermal gradients were achievable. The protocol and sequence of operations for MICAST7 were similar to those employed for MICAST6. Differences were the pre-DS period was reduced from 5 hrs. to 1 hr. and the DS had a furnace-withdrawal rate of 20 μm s^{-1} for about 8.4 cm followed by a rate of 11 μm s^{-1} for 6.5 cm. Again the outputs of the thermocouples positioned along the length of the alumina tube in the SCA were reduced to provide velocities of and thermal gradients at the liquidus and solidus isotherms during DS. The initial isotherm velocities increased to the aim-velocity of 20 μm s^{-1} over a distance of about 1.5-2.0 cm. DS at the aim-velocity of 20 μm s^{-1} was achieved for approximately 6.4-6.9 cm. The transition from the higher to the lower solidification velocity occurred over a distance of approximately 3 cm, and DS at the lower aim-velocity was over a length of about 4 cm. The thermal gradients achieved for the DS-period of MICAST7 were 26 +/- 1 ^{o}C cm^{-1} at the liquidus and 22 +/- 1 ^{o}C cm^{-1} at the solidus.

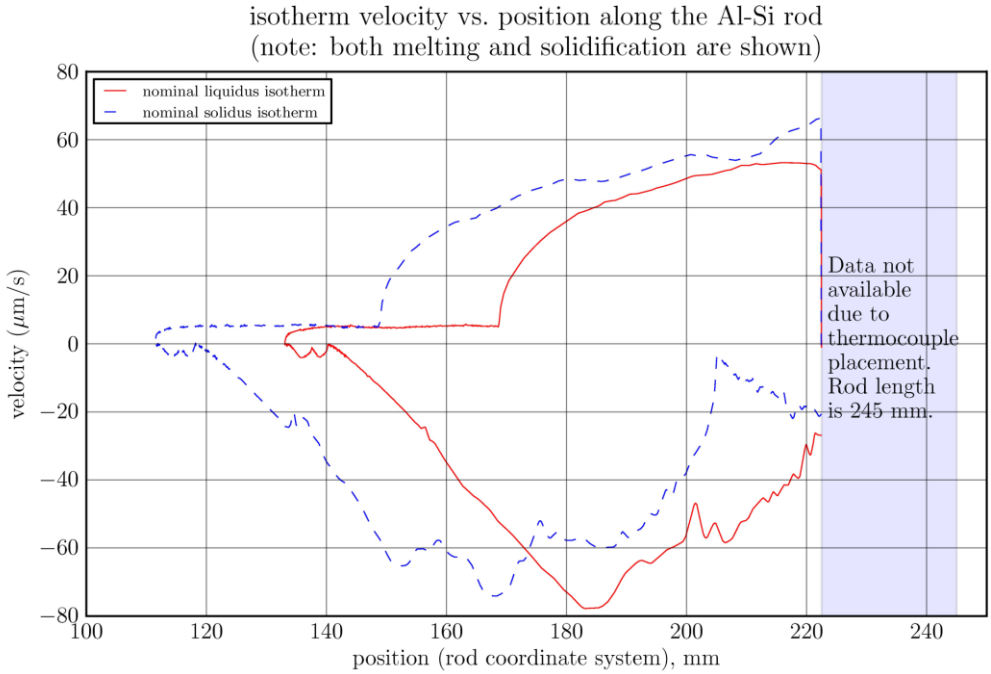

Figure 6: Liquidus-isotherm velocity (solid red curve) and solidus-isotherm velocity (broken blue curve) for MICAST6. Pre-DS has the negative velocities; the DS has positive velocities. The DS withdrawal rate was 5 μm s^{-1} for 3.8 cm and 50 μm s^{-1} for 11.3 cm.

Radial Segregation and Dendritic Metrics

A. Radial Segregation

The dendritic microstructures of two transverse sections, which were terrestrially solidified, are shown as Figs. 8(a) and 8(b). These specimens are from bars that were DS-ed under a thermal gradient of 15 ^{o}C cm^{-1}. With the solidification rate at 5 μm s^{-1} (Fig. 8(a)), there is obvious "steepling" with eutectic concentrated at the periphery at 3 o'clock and 8 to 12 o'clock. Furthermore, the secondary branching is poorly defined over much of the section. With the rate at 50 μm s^{-1} (Fig. 8(b)), there is some steepling with eutectic more concentrated along the periphery at 9 to 12 o'clock, but the dendritic structure is clearly apparent, unlike Fig. 8(a). In both cases, steepling is indicative that thermosolutal convection was present during the DS-process. That the eutectic constituent is offset somewhat could be attributed to a non-uniform temperature around the periphery. Only a small variation in temperature around the periphery is enough to drive a non-symmetrical thermosolutal pattern during DS.

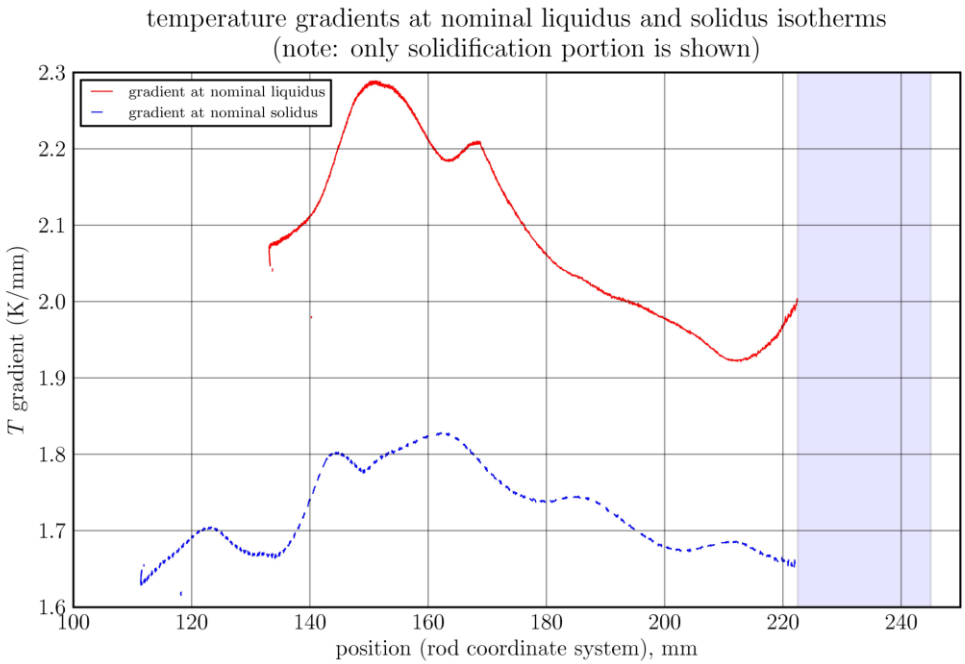

Figure 7: Thermal gradient at liquidus (red curve) and at eutectic-solidus (blue curve) for MICAST6. DS withdrawal rate 5 μm s^{-1} for 3.8 cm and 50 μm s^{-1} for 11.3 cm

Microstructures of two transverse sections taken from MICAST6, which was solidified aboard the ISS, are shown as Figs. 9(a) and 9(b). The average thermal gradient across the mushy zone was about 19 ^{o}C cm^{-1}. With the solidification rate at 5 μm s^{-1} (Fig. 9(a)), the eutectic constituent is somewhat concentrated along the upper portion of the periphery. In 0-g and no other forces driving convection, there should be no radial segregation. We attribute the mild radial-segregation to a free-surface of the liquid in the sample during its DS. When the MICAST6 sample was removed from its SCA, there was a separation of the alloy from the alumina crucible-mold. At a free-surface in a thermal gradient, there would be Marangoni convection. At the faster solidification velocity, 50 μm s^{-1} (Fig. 9(b)), no radial segregation is evident. Convection-related macrosegregation diminishes as solidification velocity increases. The sample removed from MICAST7 exhibited only a slight indication of a free surface during its DS. Thus, even at a relatively low solidification velocities of 10 and 20 μm s^{-1}, there was no radial segregation in the transverse sections examined in this study.

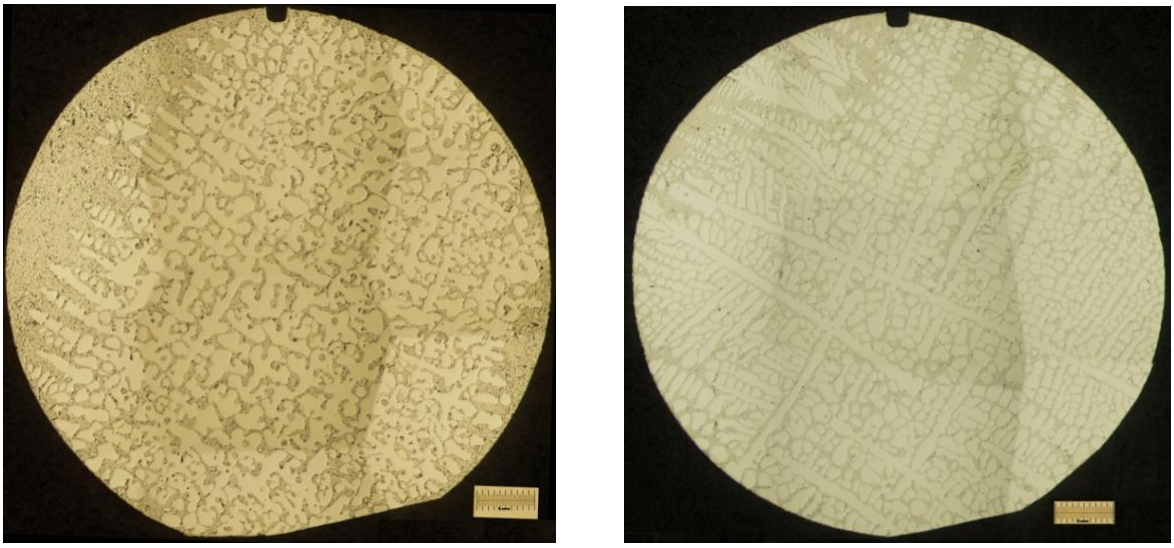

(a) **(b)**

Figure 8: Transverse sections of samples terrestrially solidified. **(a)** DS-ed at 5 μm s^{-1} with a thermal gradient of ~15 ^{o}C cm^{-1}; **(b)** DS-ed at 50 μm s^{-1} with a thermal gradient of ~15 ^{o}C cm^{-1}.

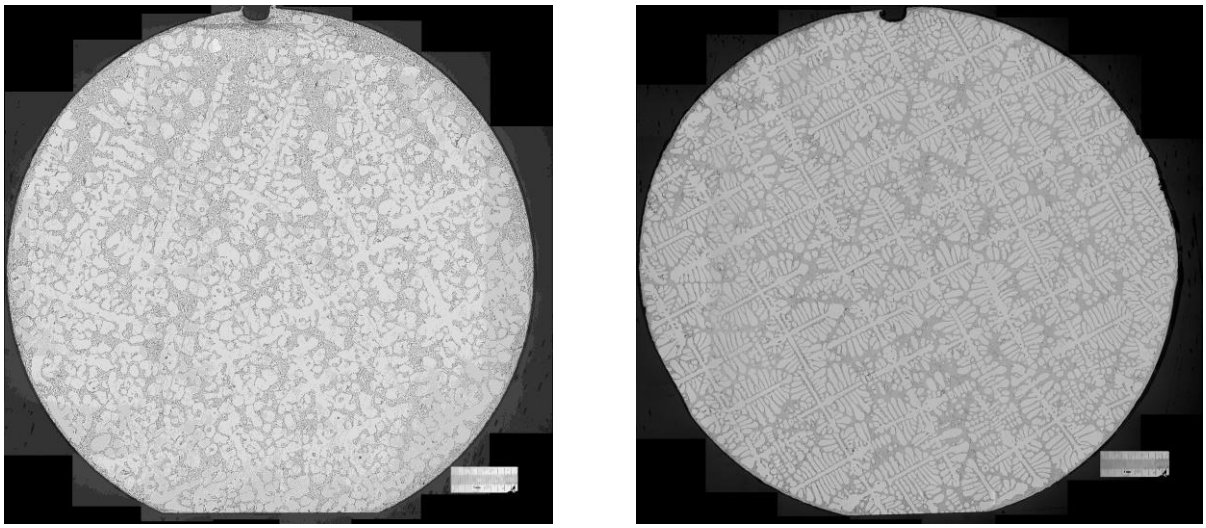

(a) **(b)**

Figure 9: Transverse specimens taken from MICAST6 DS-ed on the ISS. **(a)** DS-ed at 5 μm s^{-1} with a thermal gradient of ~20 ^{o}C cm^{-1}; **(b)** DS-ed at 50 μm s^{-1} with a thermal gradient of ~20 ^{o}C cm^{-1}

B. Dendrite Metrics

Figures 10(a) and 10(b) show features of microstructures of directionally solidified materials. Figure 10(a) is an image of the microstructure of the subject alloy, Al-7 wt.% Si, taken from a plane normal to the growth direction. Indicated in black are a primary dendrite arm spacing, λ_1, a tertiary dendrite arm spacing, λ_3, an "x" from which a measure of "trunk diameter" is obtained, and two intersecting lines along (100) of two dendritic grains in the image. In Fig. 10(b) a section parallel to the growth direction of a transparent "alloy" shows λ_1 and the trunk diameter. In this article, we report on the primary dendrite arm spacings and trunk diameters in specimens taken from MICAST6 and MICAST7 and compare/contrast these metrics to the same in terrestrially solidified samples. Measuring other dendrite-metrics is still in progress, so they are not reported in this article.

Hunt and Lu[3] devised a model for calculating the primary dendrite arm spacing, λ_1, under steady DS-growth conditions. The model assumes the transport of solute only by mass diffusion among a group of advancing primary arms. On the transverse section, dendrite tips are arranged in triangular packing, so each tip has six nearest neighbors. By numerical calculations, they observed the spacing when the solute-diffusion fields of an advancing tip and its neighbors overlapped to the extent that the diffusion in the liquid at advancing tip was not sufficient to keep up with the solute rejected at the tip. We have used their model to predict the primary dendrite arm spacing that has been measured from transverse specimens taken from MICAST6 and MICAST7 and transverse specimens from samples DS-ed terrestrially.

To be compatible with the theoretical model of Hunt and Lu[3], we measured the nearest neighbor spacings. In a transverse section, the centers of the primary dendrite arms are identified. The center-to center distances of the nearest neighbor to each center are measured. The method of accounting is done so as not to double count the distance between a pair of centers. The measured spacings of the ISS-grown and terrestrially grown samples are summarized in Fig. 11. The points are average nearest neighbor spacings, and the error bars indicate the ranges from which the averages were computed. The abscissa represents the spacing calculated from the model of Hunt and Lu[3], which apply for no convection. The line, therefore, represents perfect agreement between the calculated and measured values. The average values of λ_1 of the ISS-grown samples agree very well with the calculated values, but several of the average-coordinates of the terrestrially grown samples do not compare. In the latter group, those that were DS-ed at solidification velocities greater than 20 μm s^{-1} did not steeple; such terrestrial-coordinates also compare well with the calculated values of λ_1. It is known that solidifying at higher growth rates lessens macrosegregation in samples with uniform cross-sections. So taken collectively, the data plotted in Fig. 11 present evidence that thermosolutal convection decreases the primary dendrite arm spacing.

The other dendrite-metric reported herein is the "primary dendrite trunk diameter" or "trunk diameter." This dendrite metric has been reported in the past in only a few articles, but in the course of this research we have re-visited this particular dendritic metric[4]. By observing *in situ* transparent "alloys" undergoing DS, one can observe that the diameter of a primary dendrite arm increases from the advancing dendrite-tip diameter as one follows the trunk diameter into the mushy zone. The same was reported by Grugel[5] for DS-ed samples of hypoeutectic Al-Si alloys that were quenched in order to capture the advancing mushy zones and dendrite tips. The model used here is an extension of Kirkwood's model for the ripening of secondary dendrite arms. Mathematical details can be found in a recently published article[4] of three of the authors. The gist is the dissolution-mass of a secondary dendrite arm is deposited on the dendrite trunk.

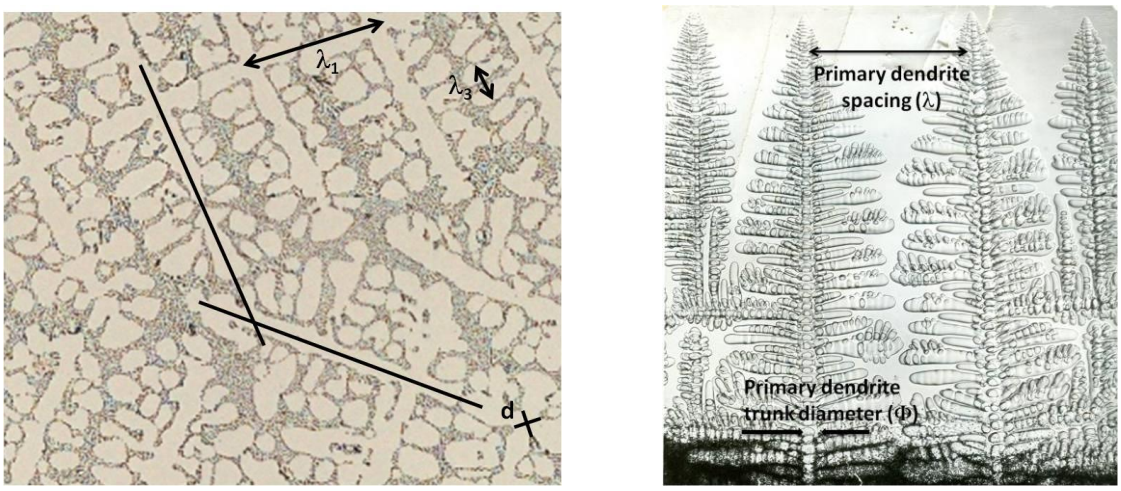

(a) **(b)**

Figure 10: Microstructures with dendrite metrics. (a) Transverse section of DS-ed Al-7Si alloy with dendrite arm-spacings, primary trunk-diameter, and two misoriented grains indicated; **(b)** transparent alloy showing primary dendrite arm spacing and dendrite trunk diameter.

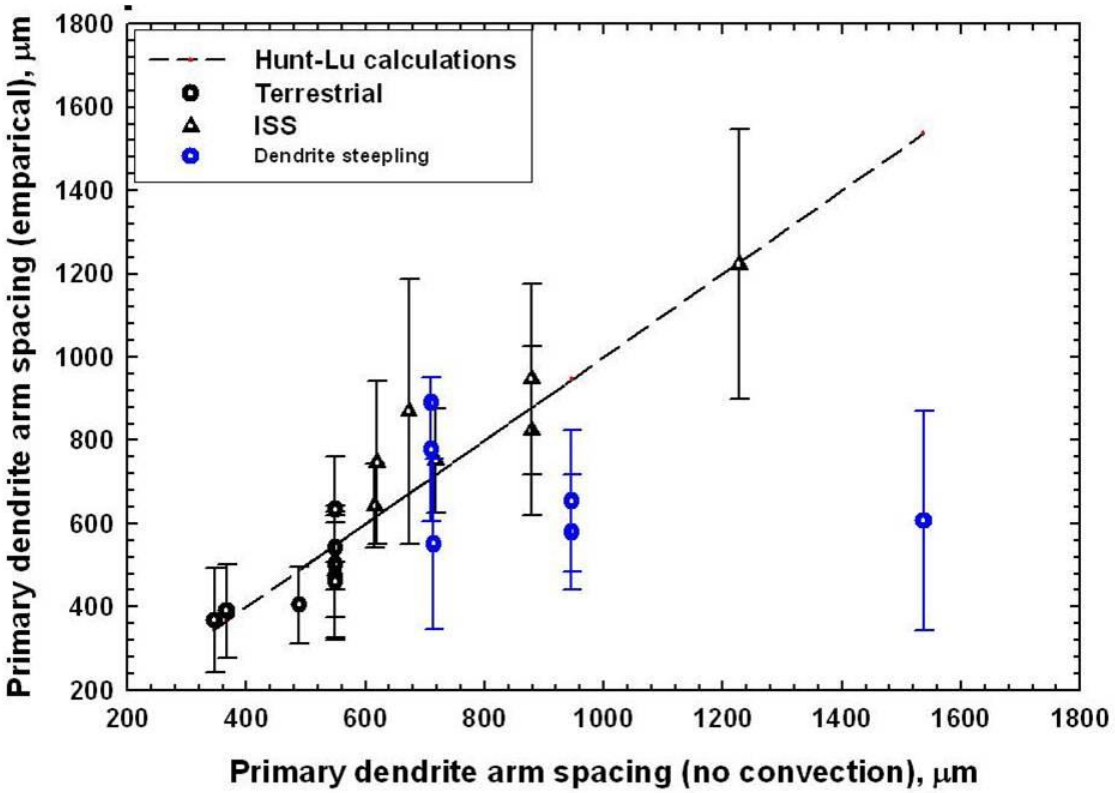

Figure 11: Measured primary dendrite arm spacings versus the same based on a diffusion controlled model (i.e., no convection).

The process is diffusion controlled, and the driving force for the diffusion in the liquid is provided by curvature/capillary differences between the positive curvature of a dissolving secondary arms and the negative curvature at the root of the arms attached to the trunk.

Our measurements are summarized as Fig. 12. Again, when the effects of thermosolutal convection are mitigated (as in high solidification velocities or in microgravity) the measured trunk diameters compare well with the model in which transport of the solute is solely by diffusion. Trunk diameters in terrestrial samples, grown at the lower solidification velocities, do not compare to the predicted values.

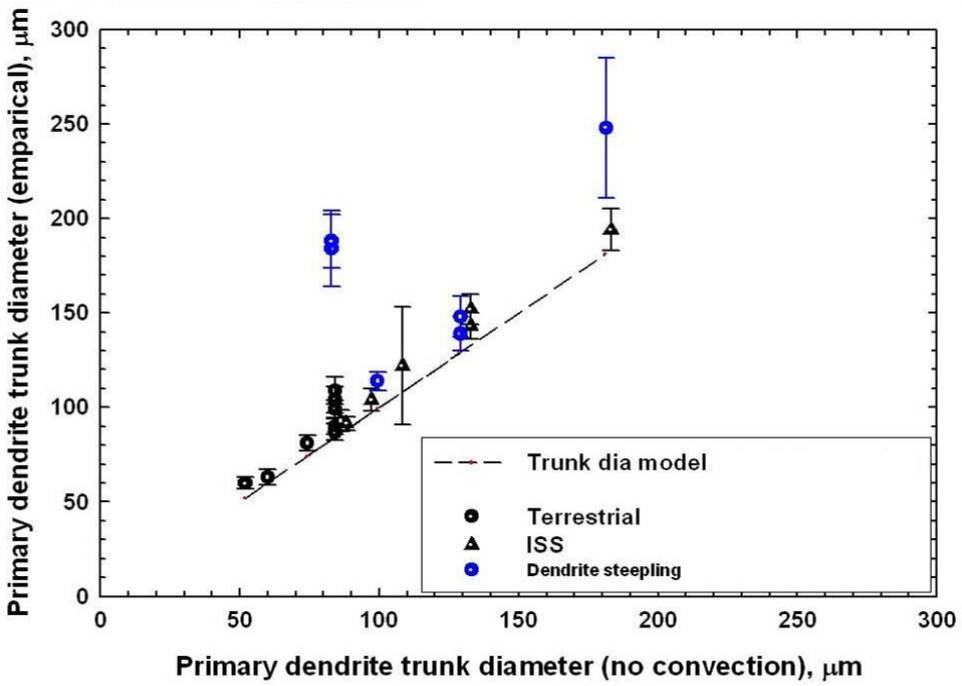

Figure 12: Measured primary dendrite trunk diameters arm versus the same based on a diffusion controlled model (i.e., no convection).

Another aspect of our research is that we have observed detached tertiary arms, even in samples with no change in cross-section. The detachment is an advanced manifestation of ripening, in which some tertiary dendrite arms remelt at their roots and detach from the main dendritic array. This suggests that the overall convection, largely buoyancy driven, is responsible for the formation of the spurious grains. Hence, space-grown samples have fewer non-uniformities in the solidified dendritic arrays than are seen in the terrestrially solidified samples. In the space-grown samples, the only convection is that associated with solidification-shrinkage and the population of spurious grains is greatly reduced. Further details have been published elsewhere[7].

Solute Redistribution during the Pre-DS Period

Here we describe and report on a diffusion-controlled process that occurs during the remelting and preparation stage prior to directional solidification (DS) of a sample on the ISS. We refer to this stage

as the pre-DE period. To effect DS on the ISS, the dendritic alloy in the SCA was partially remelted before DS commenced. During this pre-DS period, the partially melted sample is held in a thermal gradient, and the mushy zone retracts somewhat as Si diffuses from the mushy zone to the all-liquid part of the sample. This diffusion controlled process results in some macrosegregation along the length of the mushy zone and into the all-liquid zone. Here we report on the analytical measurements and the modeling and computer simulations of the longitudinal macrosegregation.

Macrosegregation has been measured by "electron microprobe analysis" (EMPA). The EMPA-analyses were used to prepare elemental X-ray maps, from which the redistribution of Si-content was determined. The elemental maps have also been used to measure the fraction of the eutectic constituent, which was used an alternative method to estimate the local Si-content. The calculated results, based on the computer model for predicting the longitudinal segregation, compare very well with the measured segregation profiles.

A. Electron Microprobe Analysis

Specimens taken from MICAST6 and MICAST 7 were analyzed using electron microprobe analysis (EMPA) on the "CAMECA SX100 Ultra," which is housed in the Department of Planetary Science at The University of Arizona. Si-K_α and Al-K_α characteristic X-rays were measured; crystals of pure Si and pure Al were used for calibration to ultimately obtain the concentrations in weight percentages. The specimens from MICAST7 and MICAST6 were prepared using standard metallographic procedures, and no etching was used. In order to avoid embedded particles from the grinding and polishing in the specimens, final polishing was done for 40 minutes on a vibratory polisher with a slurry of 0.05 μm alumina-particles. The specimens were carbon coated and analyzed in the EMPA. After numerous trials, unless otherwise specified, a beam size of 10 μm was selected for the analyses.

A preliminary EMPA-analysis was conducted at an accelerating voltage of 10 keV with a beam current of 40 nA. Drift in beam current was minimal; e.g., the longest run lasted 72 hours and the drift in the beam current was only +/- 1 nA. Elemental X-ray maps of predetermined areas were required in order to analyze an entire specimen. These maps were stitched together using a computer program called "GIMP" by overlapping the images by 20 μm[8]. Elemental X-ray maps of specimens from MICAST 6 are given as Figs. 13 and 14; lighter areas correspond to higher Al-concentrations and gray areas correspond to higher Si- concentrations in the eutectic-constituent.

Figures 13 and 14, of course, are longitudinal sections taken from MICAST6. After the sample had been removed its alumina crucible-mold in its SCA, it was carefully machined along its length to reveal its longitudinal dendritic structure. So that transverse specimens could be taken, the machined plane did not extend to the center-line. The intersection of the machined plane appears as a flat on a transverse section; the flats can be seen in Figs. 8(a) and (b) and Figs. 9(a) and 9(b). The X-ray data collected for the X-ray maps were averaged over cross-wise strips of 100 μm, so each point plotted in plots subsequently plotted is the average of all the measured EMPA-concentrations in an area of the width of the machined plane by 100 μm. Because of the diffusion of Si in the mushy zone during the pre-DS period, the nominal concentration of Al-7Si in the starting seed crystal is not maintained. Figures 13 and 14 show an obvious redistribution of Si has taken place; Figs. 15 and 16 show the measured values of the concentration of Si corresponding to Figs. 13 and 14, respectively.

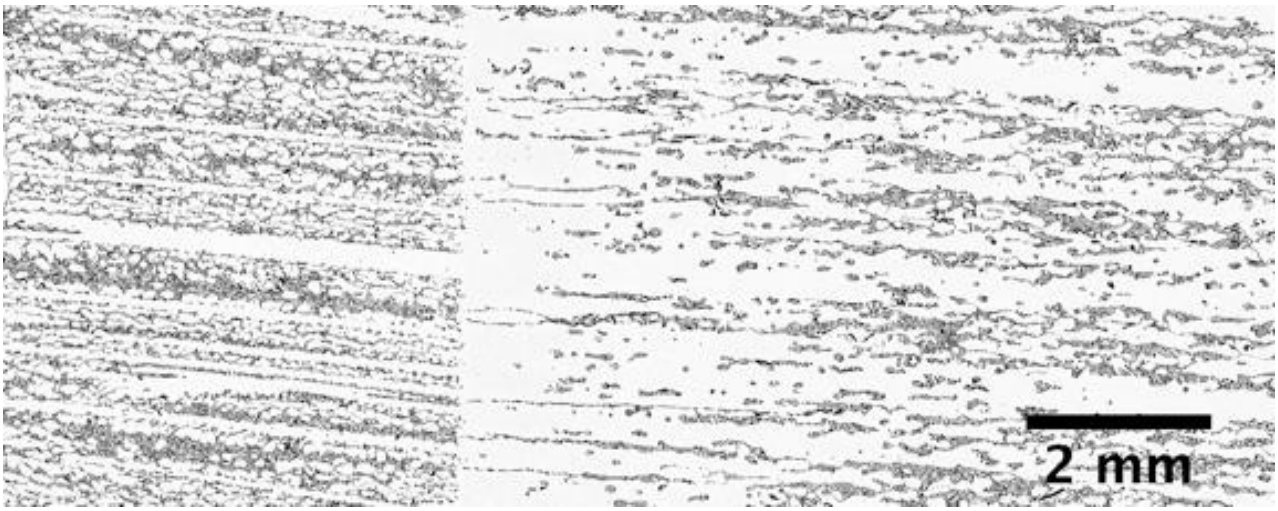

Figure 13:EMPA X-ray map of Si in MICAST6 at the beginning of the pre-DS mushy zone.

:

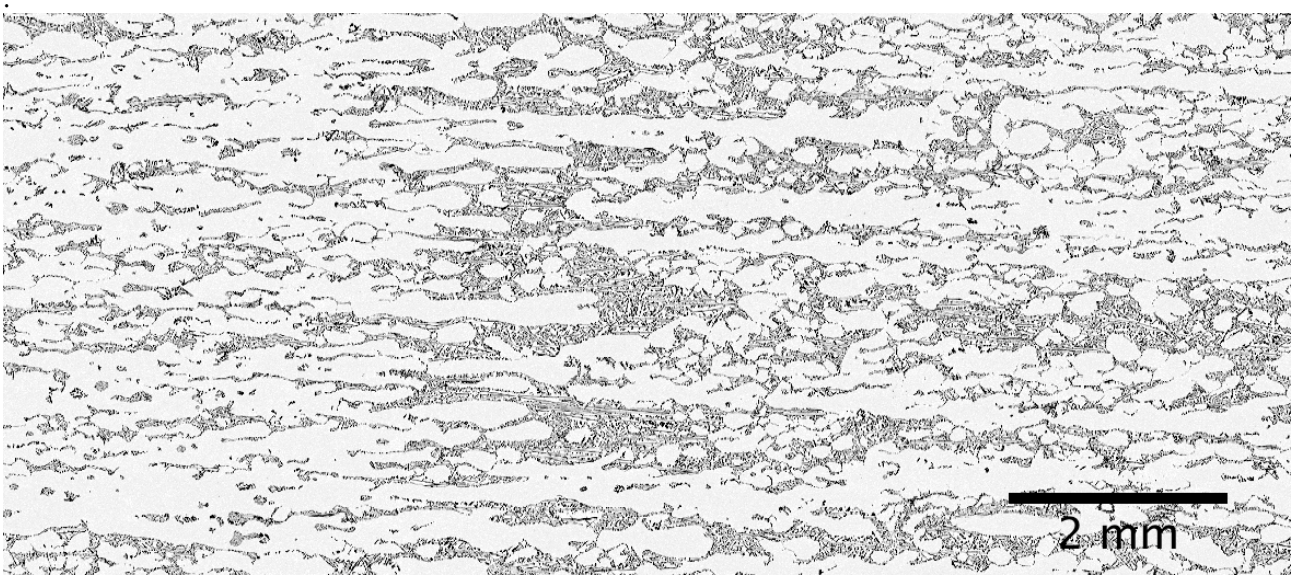

Figure 14: EMPA X-ray map of Si in MICAST6 at the end of the pre-DS mushy zone.

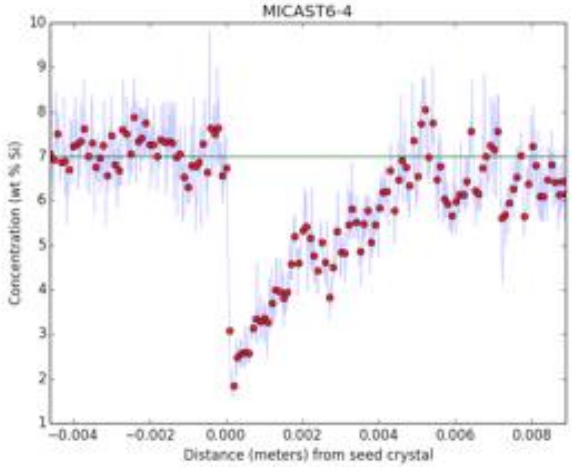

Figure 15: Plot of macrosegregation of Si in specimen MICAST 6-4, corresponding to Fig. 13. Each red dot represents an area of 100 µm x 5500 µm.

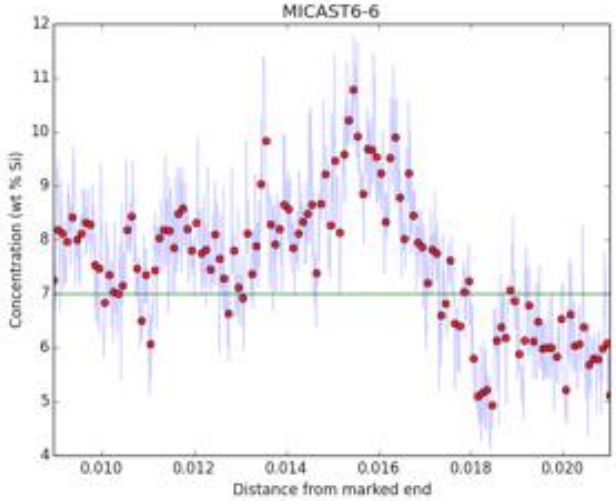

Figure 16: Plot of macrosegregation of Si in specimen MICAST 6-6, corresponding to Fig. 14. Each red dot represents an area of 100 µm x 4860 µm.

Figure 13 shows the structure of the unmelted portion of the seed crystal to the left of the white band. Part of the mushy zone that was maintained in the thermal gradient before DS commenced can be seen to the right. The thin white band, which clearly separates the unmelted portion of the seed crystal from the mushy zone, was at the eutectic temperature of the binary alloy during the pre-DS period. Figure 14 is from the same mushy-zone of MICAST6, but it is not contiguous with the area seen in Fig. 13. The area portion of the pre-DS mushy zone is seen in the leftmost third of Fig. 14. There is an obvious change in the dendritic structure at about 4 to 5 mm from the left end of Fig. 14. To the right of Fig. 14, is the

dendritic microstructure that evolved when the sample furnace was withdrawn from the furnace and DS commenced.

Similar longitudinal sections of MICAST7 were analyzed in the same manner as the specimens of the longitudinal planes MICAST6. In the next sub-section, we describe a computer-model that was devised to simulate the dynamics of the changes that occurred in the samples as they underwent the pre-DS remelting and holding.

B. *Model for Computer Simulations.*

Mathematical equations and numerical details are not presented here for the sake of brevity. The following is a description of the model, so readers can glean the major elements contained in the model. At a given isotherm/isoconcentration-plane in the mushy zone, the average Si-concentration inclusive of both phases decreases as diffusion takes place. The diffusion takes place when the solid and liquid interface tries to reach equilibrium in the temperature gradient. This interactions leads to a concentration gradient in the interdendritic liquid and thus diffusion occurs. As the solute at the eutectic isotherm lessens, a band of the primary solid is left behind. This can be clearly seen in Figs. 13 and 15. As diffusion of Si in the interdendritic liquid of the mushy zone occurs, the overall length of the mushy zone lessens. At the leading front of the mushy zone the solid becomes blunted, so there is a jump in fraction of liquid from the mushy zone into the all-liquid zone. Corresponding to this diffusional process, some macrosegregation along the length of the sample evolves. Strictly speaking, therefore, the subsequent DS is not into a liquid of uniform concentration.

The mathematical model underlying the computer simulations comprises a solute-conservation equation (i.e., the diffusion equation) with a variable diffusion coefficient in the liquid and a varying volume fraction of liquid. The model assumes no diffusion in the solid-phase, so the average concentration of solute in the solid has to be tracked with time. The phase diagram is linearized to represent the solid-liquid equilibrium between the nominal concentration and the eutectic concentration. During an ISS-experiment, the temperatures of the sample were recorded from the thermocouples on the outside of the crucible-mold (an alumina tube), so the crucible mold was included in the calculation domain. Temperatures on the outside of the crucible-mold were used as temporal and spatial boundary conditions for the energy equation. Since the experiments were carried out aboard the ISS, the very small component of the gravity was ignored, so the momentum equation was not considered. Shrinkage flow due to a change in density upon solidification was also neglected.

The finite-volume method was used to solve the governing equations with the constraint of equilibrium at the solid-liquid interface. Time steps were small enough so that the variables, including the volume fraction of liquid could be continually updated. Special care was taken when solving for the dependent variables in the numerical volumes that were at or near the discontinuity between the all-liquid volumes and the mushy zone volumes with the least fraction of solid. The thermal field was solved using the FiPy simulation package developed at NIST[9] . It was applied to a two-dimensional cylindrical mesh of the alloy sample and surrounding crucible-mold included in the domain. The diameter of the sample was 7.8 mm and the crucible-mold had a wall thickness of 1.2 mm. The mesh used for solving the diffusion equation had elements of $\Delta z = 0.0001$ m and $\Delta r = 0.0005$ m. It was found during testing of the code that the higher resolution was needed in the z-direction particularly at the tips of the dendrites that abutted the all-liquid zone. Thermal conductivities were assigned according to the phase and material:

solid-phase, liquid-phase, mushy-zone or alumina.

C. Results of Simulations

The dynamics of the changes that occur in the mushy-zones of MICAST6 is shown in Fig. 17. The upper panels in Figure 23 plot concentrations; $\overline{C}$ is the two-phase average-concentration of Si and C_l^l is the concentration of Si in the liquid. At 6460 s, the sample has been melted back, and the mushy-zone has been established. It extends from about 0.141 m to 0.165 m. This represents the condition of the sample at the beginning of the period when the sample is held for some time before DS is commenced. Hence, macrosegregation has yet to set in, which is seen by the flatness of the $\hat{C}$-curve in the top-left panel. At the same 6460 s, the volume fraction of liquid, Φ, is plotted in the left-middle panel. The jump in Φ at 0.141 m represents the fraction of eutectic liquid just when the mushy-zone has been established during pre-DS. The left-lowest panel is a plot of the temperature in the alloy sample at its center and the alloy/alumina interface. This shows that the temperature in the sample is essentially one dimensional in the *z*-direction.

The panels in the second and third rows show significant dynamic-changes of the pre-DS mushy zone at 11,460 s (a diffusion time of approx. 1.4 hrs.) and at 18,800 (a diffusion time of approx. 5 hrs.). During these periods, the one dimensionality of the system is maintained. The plots of the average concentration, $\hat{C}$, reflect that the eutectic liquid has been depleted at the mushy zone/all-solid interface and that there is a jump at the mushy zone/all-liquid interface. These dynamics, of course, can also be seen in the corresponding plots that show Φ (*z*). Between 11,640 s and 18,800 s, adjustments in the power settings of the "hot zone" were made, and the effect of these adjustments in the temperature field can be seen in the right-most panels. A similar simulation was also made for the mushy zone dynamics of MICAST7. In both simulations, the temperature in the sample was seen to be radially uniform (the three lowest panels in Fig. 17).

Beyond the times represented in Figs. 17, MICAST 6 and 7 were eventually completely solidified. Post-solidification segregation profiles are shown as Figs. 18 and 19. In Fig. 18, measured data are shown as the individual plotted coordinates. Two beam sizes, 10 μm and 14 μm, were used for the EMPA-measurements. The EMPA-measurements have been normalized such that the average of the measured concentrations in the seed crystal is 7 wt.% Si. As solidification progressed, the diffusion in the "starting" mushy zone has smoothed the segregation profile, according to the result of the simulation. The beginning of the DS is at about 0.020-0.021 m. The insert, which can be seen also as Fig. 14, clearly shows the onset of DS. The simulation-model does a very good job of predicting the segregation profile. It appears, however, that the model underestimates the gradient in the Si-concentration where DS commenced (0.0020 to 0.0265 m) on Figure 16. The model uses the mass diffusivity recommend by Poirier [10]. As discussed in that article, there are very few experimental data, and those data are probably unreliable. Hence, some of the difference between the EMPA-points and the simulation shown in Fig. 17 could be attributed to the uncertainty in the mass-diffusivity of Si in the liquid alloy. Another possibility for the differences is that the model does not include transport by advection of the very small shrinkage-driven flow. Finally, the Soret-diffusion is not included in the model. Since the thermal gradient is on the order of only 20 K cm^{-1}, then this effect is probably negligible. For post-DS MICAST7, the simulation and the EMPA-data also compare very well (Fig. 19).

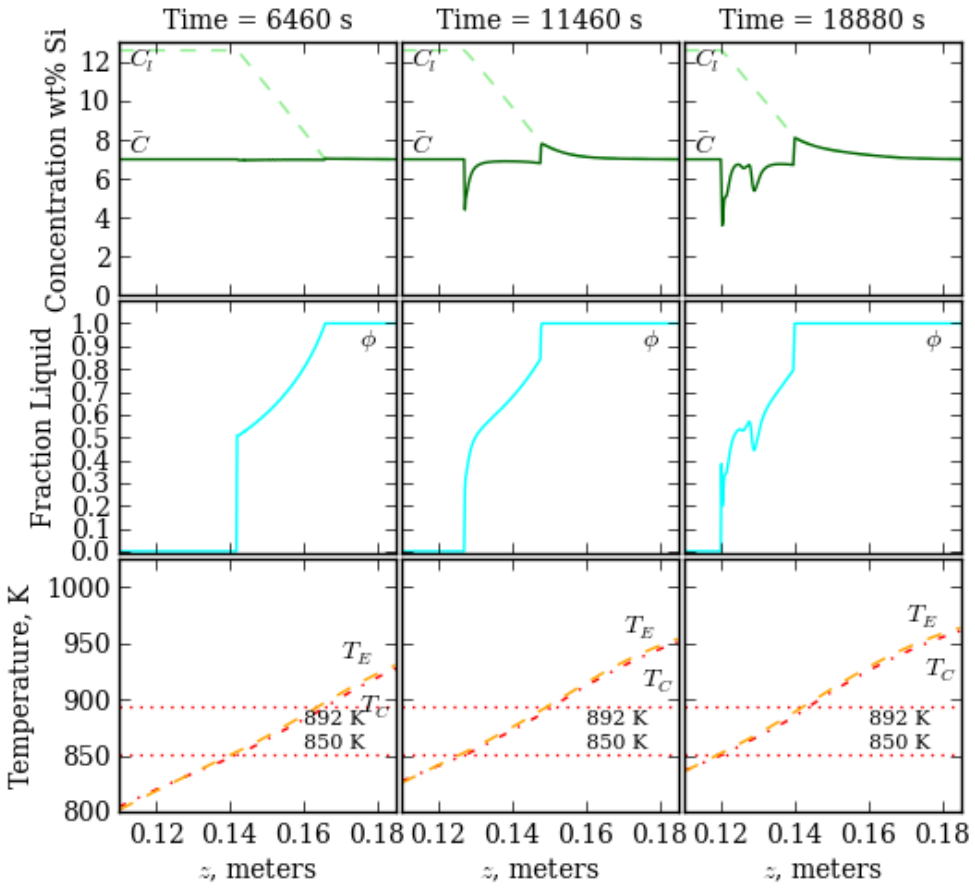

Figure 17: Dynamics of changes in the mushy zone during the pre-DS period of MICAST6. From left-to-right, the panels show concentrations at 6,460 s, 11,460 s and 18,880 s. The nominal liquidus of the alloy is 892 K and the eutectic temperature is 850 K. There is a shift in the axis in this figure, and a 0.12 meter point is the 0.0 meter point in the previous and following figures.

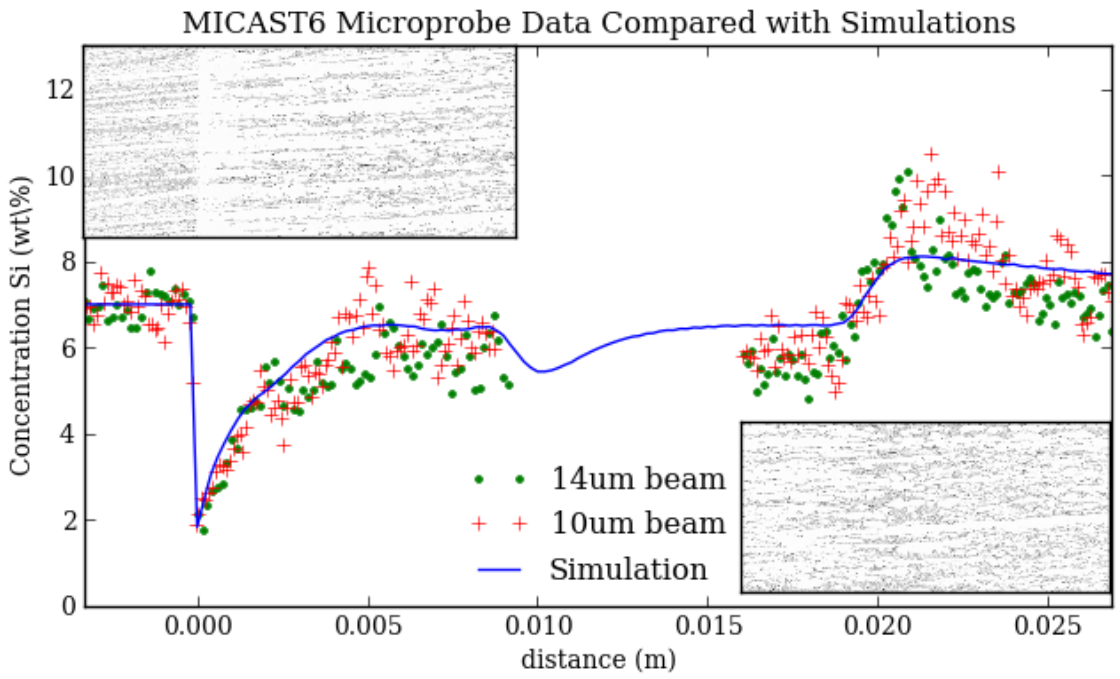

Figure 18: Macrosegregation in MICAST6 after directional solidification. The insets are elemental X-ray maps for Si that have been positioned to correspond to the plot of the concentration of Si.

Conclusions and Added Comments

Primary dendrite arm spacings of DS-ed Al-7Si alloy processed aboard the ISS, as MICAST6 and MICAST7, show good agreement with the diffusional model of Hunt and Lu[3]. Together, the scope of solidification conditions in these samples covers solidification velocities of 5 to 50 μm s^{-1} and thermal gradients of ~ 19 to 26 ºC cm^{-1}. The terrestrial samples, when grown at rapidly high solidification velocities follow the Hunt-Lu model[3] but have primary dendrite arm spacings that are much less than those predicted by the diffusional model of Hunt and Lu. It is also clear that thermosolutal convection is responsible for the steepling-type macrosegregation observed in the terrestrially grown samples that are solidified slowly.

The primary trunk diameters of the samples processed on the ISS show good agreement with our model[4], which again is a diffusion-only process and is an extension of Kirkwood's model[6] for dendrite ripening. The primary trunk diameters of the samples processed terrestrially, especially those solidified at relatively low solidification velocities, differ significantly from those calculated for diffusion-only conditions.

Using two methods based on elemental X-ray maps of Si in segregated regions of MICAST6 and MICAST7 and computer simulations based on diffusion-limited transport, we have determined the dynamics of changes and segregation that take place during pre-DS period in the LGF and SQF Bridgman-type furnaces aboard the ISS. The model used for the computer simulations successfully captured the dynamics of the structural and segregation changes that take place during the pre-DS thermal adjustment of the LGF and the SCA. The computer simulations utilize the actual temporal and spatial temperatures collected during the solidification processing on the ISS. Two-dimensional calculations of the thermal field in cylindrical coordinates showed that the radial temperature within the alloy sample, itself, is almost uniform so that a one-dimensional model of the mass diffusion captures the dynamics and segregation of the samples when

processed in a microgravity environment.

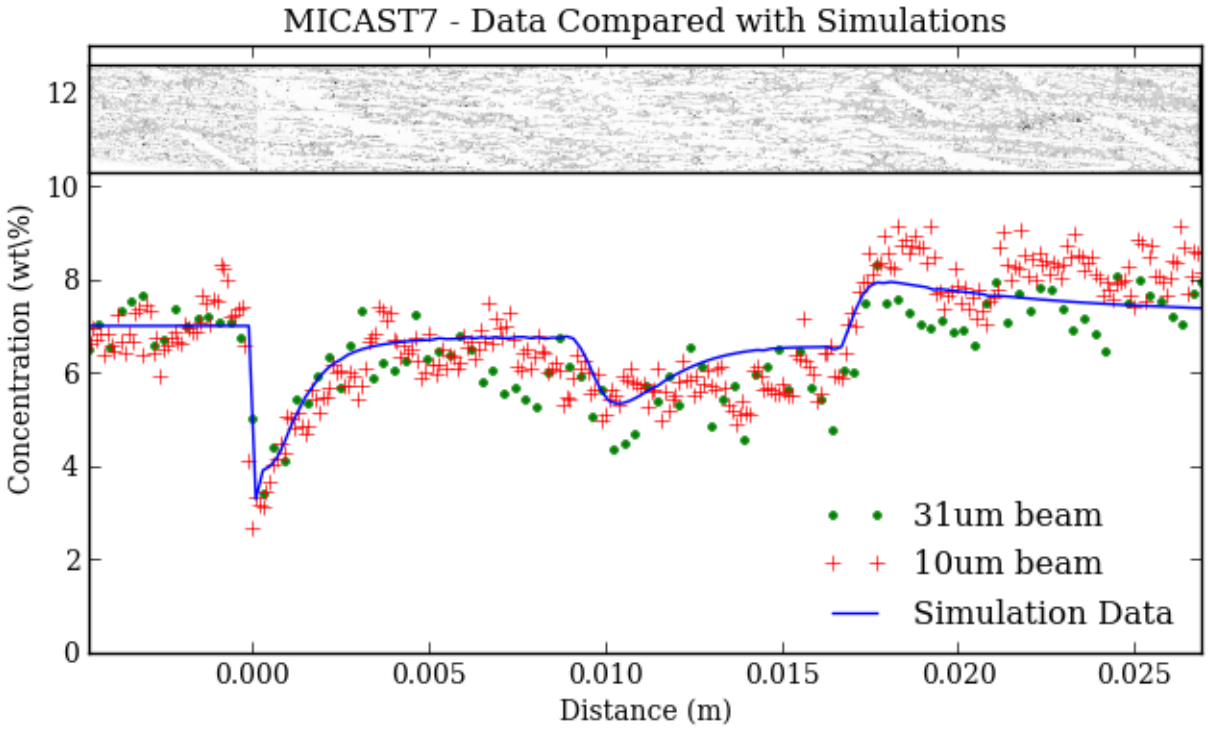

Figure 19: Macrosegregation in MICAST7 after directional solidification. The elemental X-ray map for Si is positioned to correspond to the plot of the concentration of Si.

Over the past two or three decades understanding of processing conditions leading to defects known as freckles has benefitted by modeling, computer simulations and experiments. In the same way, the current research promises to elucidate the processing conditions and alloys prone to steepling. Beyond the scope of the research of this article, we are also studying effects of alloys with differing buoyancy characteristics during DS through changes in cross-sections (both contractions and expansions). In addition to examining dendrite-metrics and macrosegregation, the research is studying the formation of spurious grains[7], particularly those sometimes found at sectional changes. The present grant and the newer grant should provide further fundamental underpinnings for the production of DS-columnar castings and dendritic mono-crystals used in gas turbine engines.

Acknowledgements

This grant has been supported by NASA Grant NNX08AN49G. Protocol of the ISS-experiments has been handled mainly by ESA-engineers and scientists and Prof. R.G. Erdmann at The University of Arizona. Scientists and engineers at NASA-MSFC assisted immensely in coordinating with ESA, real-time communications during the space experiments and arranging for return of the ISS-processed samples to earth. Prof. Erdmann also devised the coding to reduce the voluminous thermocouple data from the ISS.

Appreciation is expressed to Dr. Men G. Chu at the ALCOA Technical Center for preparing the alloys and to the Materials and Processing Laboratory at MSFC for allowing one of the authors (R.N. Grugel) to devote some of his time to this project.

References

1. T. Huang, S. Liu, Y. Yang, D. Lu and Y. Zhou: "Coupling of Couette flow and crystal morphologies in directional solidification," *J. Cryst. Growth* **128**, 1993, 167-172.

2. M.D. Dupouy, D. Camel and J.J. Favier:"Natural convection effects in directional dendritic solidification of binary metallic alloys: dendritic array primary spacing," *Acta Met. Mater.* **40** (7), 1992, 1791-1801.

3. J.D. Hunt and S.-Z. Lu:"Numerical Modeling of Cellular/Dendritic Array Growth:Spacing and Structure Predictions," *Metall. Trans.* **27,** 1996, 611-623.

4. S.N. Tewari, R.N. Grugel, and D.R. Poirier: "An evaluation of primary trunk diameters in directionally solidified Al-Si alloys," *Metall. Mater. Trans. A* **45A**, 2014, 4758-4761.

5. R.N. Grugel: "Microstructural evolution of primary dendrite trunks in directionally solidified, hypoeutectic aluminum- silicon alloys,"*Metall. Mater. Trans. A* **26A**, 1995, 496-499.

6. D.H. Kirkwood: "A simple model for dendrite arm coarsening during solidification," *Mat. Sci. Eng.* **73**, 1985, L1-L4.

7. J.R. Van Hoose, R.N. Grugel, S.N. Tewari, L.N. Brush, R. Erdmann and D.R. Poirier: "Observation of mis-oriented tertiary dendrite arms during controlled directional solidification in aluminum-7 wt% silicon alloys," *Metall. Mater. Trans. A* **43A**, 2012, 4724-4731.

8. S. Kimball and P. Mattis: GNU Image Manipulation Program, *GIMP 2.810,* 2013, www.gimp.org.

9. J.E. Guyer, D. Wheeler and J.A. Warren: "FiPy: Partial Differential Equations with Python,"*Comput. Sci. Eng.* **11,** 2009, 6-15.

10. D.R. Poirier: "Density, viscosity, and diffusion coefficients in hypoeutectic Al-Si liquid alloys: an assessment of available data," *Metall. Mater. Trans. B* **45B**, 2014, 1345-1354. http://www.springerlink.com/openurl.asp?genre=article&id=doi:10.1007/s11663-014-0037-8.